



Turbulent length scales and budgets of Reynolds stress-transport for open-channel flows; friction Reynolds numbers (R_{τ})=150, 400 and 1020

DOI:

[10.1080/00221686.2020.1729265](https://doi.org/10.1080/00221686.2020.1729265)

Document Version

Final published version

[Link to publication record in Manchester Research Explorer](#)

Citation for published version (APA):

Ahmed, U., Apsley, D., Stallard, T., Stansby, P., & Afgan, I. (2020). Turbulent length scales and budgets of Reynolds stress-transport for open-channel flows; friction Reynolds numbers (R_{τ})=150, 400 and 1020. *Journal of Hydraulic Research*, 1-15. <https://doi.org/10.1080/00221686.2020.1729265>

Published in:

Journal of Hydraulic Research

Citing this paper

Please note that where the full-text provided on Manchester Research Explorer is the Author Accepted Manuscript or Proof version this may differ from the final Published version. If citing, it is advised that you check and use the publisher's definitive version.

General rights

Copyright and moral rights for the publications made accessible in the Research Explorer are retained by the authors and/or other copyright owners and it is a condition of accessing publications that users recognise and abide by the legal requirements associated with these rights.

Takedown policy

If you believe that this document breaches copyright please refer to the University of Manchester's Takedown Procedures [<http://man.ac.uk/04Y6Bo>] or contact uml.scholarlycommunications@manchester.ac.uk providing relevant details, so we can investigate your claim.





Turbulent length scales and budgets of Reynolds stress-transport for open-channel flows; friction Reynolds numbers (Re_τ) = 150, 400 and 1020

Umair Ahmed, David Apsley, Timothy Stallard, Peter Stansby & Imran Afgan

To cite this article: Umair Ahmed, David Apsley, Timothy Stallard, Peter Stansby & Imran Afgan (2020): Turbulent length scales and budgets of Reynolds stress-transport for open-channel flows; friction Reynolds numbers (Re_τ) = 150, 400 and 1020, Journal of Hydraulic Research, DOI: [10.1080/00221686.2020.1729265](https://doi.org/10.1080/00221686.2020.1729265)

To link to this article: <https://doi.org/10.1080/00221686.2020.1729265>



Published online: 03 Apr 2020.



Submit your article to this journal [↗](#)



View related articles [↗](#)





View Crossmark data [↗](#)





Forum paper


Turbulent length scales and budgets of Reynolds stress-transport for open-channel flows; friction Reynolds numbers (Re_τ) = 150, 400 and 1020

UMAIR AHMED , Lecturer, School of Engineering, Newcastle University, Newcastle upon Tyne NE1 7RU, UK
Email: umair.ahmed@newcastle.ac.uk

DAVID APSLEY , Lecturer, School of Mechanical, Aerospace and Civil Engineering, University of Manchester, Manchester M13 9PL, UK
Email: d.apsley@manchester.ac.uk

TIMOTHY STALLARD , Professor, School of Mechanical, Aerospace and Civil Engineering, University of Manchester, Manchester M13 9PL, UK
Email: tim.stallard@manchester.ac.uk

PETER STANSBY , Professor, School of Mechanical, Aerospace and Civil Engineering, University of Manchester, Manchester M13 9PL, UK
Email: p.k.stansby@manchester.ac.uk

IMRAN AFGAN , Associate Professor, Department of Mechanical Engineering, School of Engineering, Khalifa University of Science and Technology, Abu Dhabi PO Box 127788, UAE; Senior Lecturer, School of Mechanical, Aerospace and Civil Engineering, University of Manchester, Manchester M13 9PL, UK
Emails: imran.afgan@ku.ac.ae, imran.afgan@manchester.ac.uk (author for correspondence)

ABSTRACT

Turbulence in open channel flows is ubiquitous to hydro-environmental applications and has recently increased in importance with the deployment of tidal stream turbines, as turbulence impacts both the turbine performance and the blade fatigue life. Tidal turbine analysis requires fully developed turbulence characteristics at the inlet of numerical simulations where generally the length scale information is limited. In this study, fully resolved large eddy simulations (LES) with flat beds were undertaken using an open source code at friction Reynolds numbers (Re_τ) of 150, 400 and 1020. It was found that the effects of the free surface on turbulence length scales were felt in approximately the uppermost 10% of the channel only, although the influence on Reynolds stresses extended further downwards. Furthermore, the cross-correlation length scales of both streamwise and spanwise velocities were found to be significantly affected by the free surface where turbulent eddies were flattened to the two-component limit.

Keywords: Anisotropy; budgets; open-channel flow; tidal stream turbines; turbulence length scales; turbulence spectra

1 Introduction

Turbulence near shear-free, approximately-flat surfaces occurs in a wide variety of industrial and environmental flows, and studying the structure of turbulence near the free surface is important for understanding the complex interaction of the gas-liquid interface. In engineering problems these flows occur in marine-energy applications, ship hydrodynamics, heat-film

exchanges, heat and momentum transfer for two-phase flows, weirs, spillways, sluices, etc. In the case of marine applications, such as tidal-stream turbines, it is important to understand the development of turbulent structures and their influence on the rest of the flow field, as the performance of, and fatigue loading on, marine energy extraction devices is directly dependent on the onset levels of turbulence. Furthermore, understanding the effects of a shear-free surface on turbulence is of fundamental

Received 1 March 2019; accepted 2 February 2020/Currently open for discussion.

importance for turbulence modelling, as models capable of predicting second-order statistics near a free surface are widely used in industrial computational fluid dynamics (CFD).

Previous experimental studies by Komori, Ueda, Ogino, and Tokuro (1982), Komori, Murakami, and Ueda (1989), Nezu and Rodi (1986), Rashidi and Banerjee (1988) and Kumar, Gupta, and Banerjee (1998) have established the behaviour of root-mean-squared (rms) velocity fluctuations in the vertical direction for open-channel flows. These experiments reported that the fluctuations in the vertical direction were damped, whereas fluctuations in the tangential direction were enhanced near the free surface. Komori et al. (1989); Nakagawa and Nezu (1981); Rashidi and Banerjee (1988) have also already established the connection between the bursts generated near the bed of the channel and the coherent motion also known as surface-renewal motion. On the other hand the effects of Reynolds-stress anisotropy have been studied experimentally by Roussinova, Balachandar, and Biswas (2009). Thus, a wealth of information regarding open-channel flows has already been provided by experiments; however, there are some difficulties related to measurements very close to the deformable interface at the free surface. This results in a lack of accuracy of measurements for the *rms* velocities near the free surface and derived quantities such as Reynolds stresses, vorticity and turbulent dissipation, all of which cannot be obtained with accuracy.

Open-channel flows have been studied via direct numerical simulation (DNS) by Komori et al. (1993), Handler, Swean, Leighton, and Swearingen (1993), Handler, Swearingen, Swean, and Leighton (1991), Borue, Orszag, and Staroselsky (1995), Lam and Banerjee (1992), Walker, Leighton, and Garzaros (1996) and Campagne, Cazalbou, Joly, and Chassaing (2009). The main limitation of these studies has been the relatively small Re numbers (when defined in terms of the depth profile). At such low Re numbers the viscous effects from the lower friction bed extend much further up into the water column; in some cases even up to the free surface. Furthermore, under these flow conditions the thickness of the viscous sub-layer forms a significant portion of the integral length scale. Consequently, it becomes difficult to distinguish between inviscid and viscous processes near the free surface (Calmet & Magnaudet, 2003). In order to study higher Re number flows, large eddy simulations (LES) for open-channel flows have been performed by Hinterberger, Fröhlich, and Rodi (2008), Taylor, Sarkar, and Armenio (2005), Calmet and Magnaudet (2003), Salvetti, Zang, Street, and Banerjee (1997) and Walker, Tejada-Martínez, Martinat, and Grosch (2014). These studies have investigated a range of friction Reynolds numbers ($Re_\tau \approx 170 - 1280$) and have explored the effects of a free surface on turbulence with and without variations in temperature. However, the present work differs substantially from the earlier studies by simulating a range of Re numbers, obtaining full budgets of the Reynolds stress equations, and deriving profiles of integral correlations and turbulent length scales that are vital for the synthesis of realistic turbulence in marine applications.

We also use higher streamwise and spanwise resolutions and larger domain sizes than all of the aforementioned numerical studies. As part of the validation work we compare our mean velocity profiles with those of Taylor et al. (2005), Yokojima and Shima (2010) and Nezu and Rodi (1986).

The main focus of this paper is to determine the variations of the turbulent length scales and the Reynolds stresses in a fully-developed open-channel flow over a range of Re numbers, as these differences have implications on the performance and efficiency of marine energy conversion devices (Ahmed, Apsley, Afgan, Stallard, & Stansby, 2017). In the current paper we thus provide the Reynolds-stress profiles, integral length scales and turbulent spectra at different Re numbers. Furthermore, the anisotropy of the Reynolds stresses are explored and to identify the key processes, the budgets for the Reynolds-stress transport equation are also presented.

The paper is arranged as follows. Section 2 describes the mathematical background and the methods used for simulating open-channel flows along with the flow configuration and the implemented numerical procedures. Section 3 presents the results for all the studied cases. Finally the conclusions are summarized in the last section.

2 Numerical procedure and flow geometry

2.1 Large-eddy simulation equations

In this paper turbulence is closed by using the LES approach. In this method the spatially-filtered incompressible Navier–Stokes equations are solved as:

$$\frac{\partial \tilde{u}_i}{\partial x_i} = 0 \quad (1)$$

$$\frac{\partial \tilde{u}_i}{\partial t} + \frac{\partial \tilde{u}_i \tilde{u}_i}{\partial x_j} = -\frac{1}{\rho} \frac{\partial \tilde{p}}{\partial x_i} + \nu \frac{\partial^2 \tilde{u}_i}{\partial x_j \partial x_j} + \frac{1}{\rho} \frac{\partial \tau_{ij}}{\partial x_j} \quad (2)$$

where $\tilde{\cdot}$ signifies space-filtered quantities. In the above equations τ_{ij} represents the sub-grid-scale (SGS) stress tensor and needs to be closed. Here, the original Smagorinsky (1963) model is used, where μ_{sgs} represents the SGS viscosity defined as $\mu_{sgs} = \rho (2C_{sgs} \Delta)^2 (2\tilde{S}_{ij}\tilde{S}_{ij})^{0.5}$, where Δ is the filter width, which is calculated as $(cell\ volume)^{1/3}$, and C_{sgs} is the Smagorinsky constant. Here, the recommended value of $C_{sgs} = 0.065$ for channel flows is used, along with Van-Driest damping near the bottom wall (Jarrin, Benhamadouche, Laurence, & Prosser, 2006). A similar formulation has been used in the LES of open channel flows by Hinterberger et al. (2008). In order to calculate fluctuating velocity for Reynolds-averaged statistics, the resolved component of the instantaneous quantities is used, $\mathbf{u}' = \tilde{\mathbf{u}}_i - \bar{\tilde{\mathbf{u}}}_i$, where the overbar indicates time averaging. Note that since the grid is highly resolved, the sub-grid scale contributions remain very small in all the current simulations. For the two-point correlations, the correlation tensor is defined as; $R_{ij}(\mathbf{r}) = \overline{(\mathbf{u}'_i(\mathbf{x})\mathbf{u}'_j(\mathbf{x} + \mathbf{r}))} / \sqrt{\overline{u'^2_i} \overline{u'^2_j}}$, where the

primes denote the fluctuating quantities and \mathbf{r} is the vector joining the two points. The corresponding length scales can then be obtained by integrating R_{ij} as $L_{ij} = \int_0^\infty R_{ij}(\mathbf{r})d\mathbf{r}$. Similar techniques have been used to estimate length scales in the past by Handler et al. (1993, 1991) for open-channel flows, Sillero, Jiménez, and Moser (2014) for turbulent boundary layers and Kim, Moin, and Moser (1987) for computing two-point correlations for a channel-flow calculation.

The calculations for this work have been performed using the unstructured finite-volume code, *Code_Saturne* (Archembaeu, Mechtoua, & Sakiz, 2004). This code has previously been used in several studies ranging from simulations of incompressible flows to low-Mach-number variable-density reacting flows (Ahmed & Prosser, 2018; Jarrin, Prosser, Uribe, Benhamadouche, & Laurence, 2009). The code solves the Navier–Stokes equations for Newtonian incompressible flows with a fractional-step method based on a prediction-correction algorithm for pressure/velocity coupling (SIMPLEC) and a Rhie and Chow interpolation to avoid pressure oscillations. In the case of LES calculations, the code uses a second-order central differencing scheme for spatial gradients; time integration is performed by a Crank–Nicholson scheme. For stability of the solution, time steps during the simulations are set such that the maximum CFL number remains below 1.

2.2 Flow configuration

The geometry of the open channels considered here is shown in Fig. 1, where the flow is driven by a uniform pressure gradient aligned with the x axis, in which turbulence is fully developed. The flow is assumed to be periodic in both axial (x) and transverse (z) directions. It can be shown by an overall momentum balance that the average pressure gradient is directly related to the averaged shear stress ($\rho \mathbf{u}_\tau^2$) as $-\partial \bar{p} / \partial x = \rho \mathbf{u}_\tau^2 / h$, where $\mathbf{u}_\tau = \sqrt{\tau_w} / \rho$ is the friction velocity, and $\tau_w = \mu (\partial \tilde{u} / \partial y)_{y=0}$ is the bed shear stress. A no-slip condition is applied at the wall on the bottom of the domain ($y = 0$), while an undeformed-surface, no-stress condition is enforced on the instantaneous velocities at the top ($y = h$) of the domain $\tilde{S}_{12} = \tilde{S}_{23} = 0$ and $\tilde{u}_2 = 0$. Here the subscripts 1, 2 and 3 correspond to x , y and z directions respectively. These boundary conditions are a good approximation for low-Froude-number flows (Calmet & Magnaudet, 2003; Hinterberger et al., 2008; Taylor et al., 2005).

Open-channel flows at three different Reynolds numbers (based on the friction velocity $R_{e\tau} = \mathbf{u}_\tau h / \nu$) have been studied

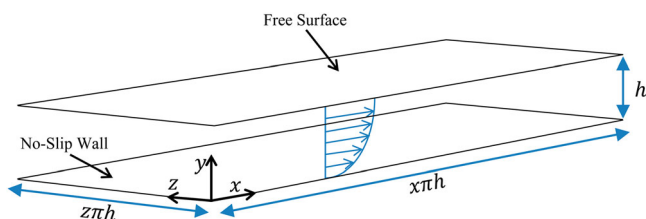


Figure 1 Model domain and coordinate system

Table 1 Domain size and mesh resolution for all cases*

$R_{e\tau}$	Domain size	Grid resolution	Δx^+ , Δy^+ , Δz^+
150	$6\pi \times 1 \times 2\pi$	$192 \times 40 \times 192$	14.7, 0.4–2.9, 4.9
400	$5\pi \times 1 \times 1.5\pi$	$320 \times 64 \times 320$	19.6, 0.4–5.5, 5.9
1020	$4\pi \times 1 \times \pi$	$396 \times 96 \times 396$	32.4, 0.5–6.2, 8.0

* All dimensions given in units of channel height h .

Table 2 Non-dimensional large-eddy turnover time, sampling time (interval between two samples) and output frequency (data write frequency)

$R_{e\tau}$	Large-eddy turnover time	Sampling time* (t_τ)	Output frequency*
150	0.0067	50	50
400	0.0025	20	100
1020	0.00098	10	200

* All data reported in non-dimensional quantities.

as listed in Table 1. Note that several combinations for the length and the width of the channels have been simulated at all $R_{e\tau}$ values, and the values reported in Table 1 lead to domain sizes that are sufficient for the two-point correlation coefficient to go to zero for the respective R_e number (more details on two-point correlations are provided in Section 3.3). All the Δx^+ , Δy^+ and Δz^+ values are below 40, which implies that the LES calculations have been performed at acceptable resolutions (Pope, 2000). This can be further verified from the velocity spectra presented in Section 3.

A hyperbolic stretching function is applied to grid points in the vertical direction, which ensures the same high level of resolution near both the free surface and the bottom wall for all the calculations.

Once a statistically-steady state was reached, the data from all the simulations were sampled at the frequencies shown in Table 2, where the non-dimensional time was defined as $t_\tau = t \mathbf{u}_\tau / h$. It can also be observed from the Table 2 that the sampling frequency for a given simulation increases as the large-eddy turnover time (LETOT) decreases. This was done to ensure that the sampling does not introduce any bias into the temporal statistics. The sampled data were then used to calculate the turbulent correlations. The simulations for $R_{e\tau} = 150$, 400 and 1020 were sampled for a total of 50, 20 and 10 non-dimensional time units respectively. The mean quantities were then obtained by averaging over all snapshots in time and in the periodic directions.

3 Results and discussion

3.1 Validation and comparison with earlier studies

Grid sensitivity studies for all the cases were performed with grids of different sizes and aspect ratios (half the grid size in

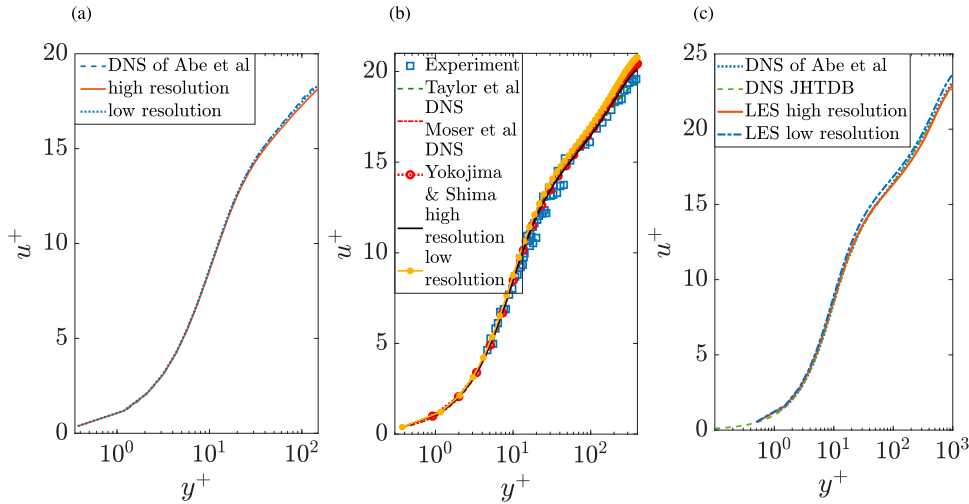


Figure 2 u^+ vs y^+ plots for different Re_{τ} values: (a) $Re_{\tau} = 150$, (b) $Re_{\tau} = 400$, (c) $Re_{\tau} = 1020$

all directions referred to as low resolution and double the grid size in all directions referred to as high resolution); it was found that the mean velocity and Reynolds stresses were not affected by these changes. It was further observed that the mean-velocity statistics at the tested Re numbers were not significantly affected by the existence of the free surface, as shown in Fig. 2.

Figures 2a and 2c show the comparison of the present open-channel flow calculations at $Re_{\tau} = 150$ and $Re_{\tau} = 1020$ with literature for fully developed channel flow with no-slip walls (Abe, Kawamura, & Matsuo, 2004)¹ and (Graham et al., 2016)² (the Johns Hopkins turbulence database (JHTDB)). On the other hand Fig. 2b shows the results for the present calculations with the DNS of Yokojima and Shima (2010) at $Re_{\tau} = 395$, LES of Taylor et al. (2005) at $Re_{\tau} = 400$ and experiment of Nezu and Rodi (1986) at $Re_{\tau} = 439$ for an open-channel flow. Furthermore, the $Re_{\tau} = 400$ case has also been compared with the DNS of Moser, Kim, and Mansour (1999)³ at $Re_{\tau} = 395$ for a full channel flow. In the $Re_{\tau} = 400$ case, a longer domain size and a higher grid resolution has been used than the earlier work of Taylor et al. (2005). It can be seen from Fig. 2a that for $Re_{\tau} = 150$ there is a slight deviation from the full channel flow beyond y^+ of 30 due to the presence of a free surface. In the case of $Re_{\tau} = 400$, a good agreement for u^+ can be seen between the present study, experimental data and the earlier studies of Taylor et al. (2005) and Yokojima and Shima (2010).

In Fig. 2c there is also a good agreement between the present study and the DNS results of Abe et al. (2004) and Graham et al. (2016). This implies that at higher Re numbers the mean velocity statistics near the free surface are similar to those in the middle of a full channel flow. Further comparisons between the Reynolds stresses of open channel and full channel flows are presented in Section 3.5.

For all the three cases the grid spacing near the wall and the free surface was smaller than the Kolmogorov scale in the vertical direction, which ensured appropriate resolution of the flow field. The bulk velocity (u_b) and skin-friction coefficient C_f are

Table 3 Bulk velocity and skin friction coefficient for different Re_{τ} values

Re_{τ}	Bulk velocity (u_b/u_{τ})	Skin friction coefficient C_f
150	15.24	8.594×10^{-3}
400	17.25	6.710×10^{-3}
1020	19.90	5.054×10^{-3}

presented in Table 3 for all the cases, where u_b and C_f are calculated as $u_b = (1/h) \int_0^h \bar{u} dy$ and $C_f = (2\tau_w)/(\rho u_b^2)$, respectively. It was found that the skin friction coefficient decreases with increasing Re number, which is consistent with the findings of Taylor et al. (2005).

3.2 Turbulent structures from mean velocities

The wall layer streaks for the open channel flow cases are shown with the help of plots of the instantaneous streamwise velocity (u/\bar{u}) at $y^+ \approx 1$ in Fig. 3. These streamwise streaks are indicators of quasi-streamwise-oriented vortices (Handler et al., 1993, 1991) and as such decrease in size with increasing Re number. The streaks periodically lift off from the wall and become unstable, eventually breaking down, leading to what are known as turbulent bursts; accounting for up to 70–80% of the production of turbulence (Brodkey, Wallace, & Eckelmann, 1974; Kline, Reynolds, Schraub, & Runstadler, 1967; Nakagawa & Nezu, 1981). In open channel flows the streaks are larger, more frequent and persist farther from the wall compared to a closed channel flow (Handler et al., 1993, 1991).

In this work we investigate this behaviour for different Re_{τ} values via visualization of instantaneous velocity from the LES data and compare near-wall velocity structures with those at mid-channel and near the stress-free upper boundary. Figures 3–5 show that the streak size decreases with increasing y/h for all Re numbers. The coherent structure of the streaks can be seen up to $y/h \approx 0.5$ in all cases. Beyond this height,

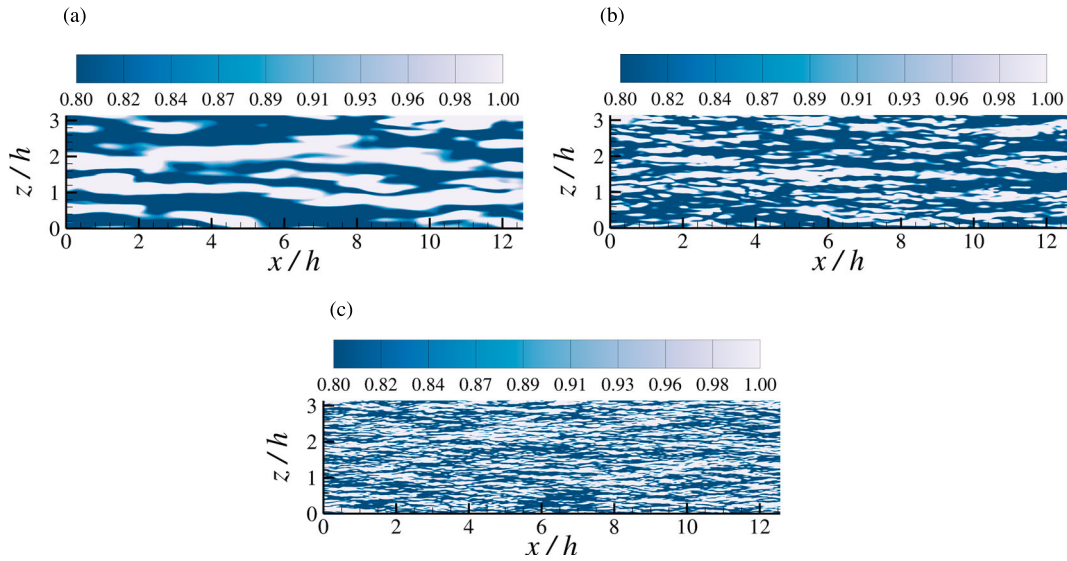


Figure 3 Instantaneous velocity (u/\bar{u}) contours close to the bottom wall for different Re_τ values: (a) $Re_\tau = 150$, (b) $Re_\tau = 400$, (c) $Re_\tau = 1020$

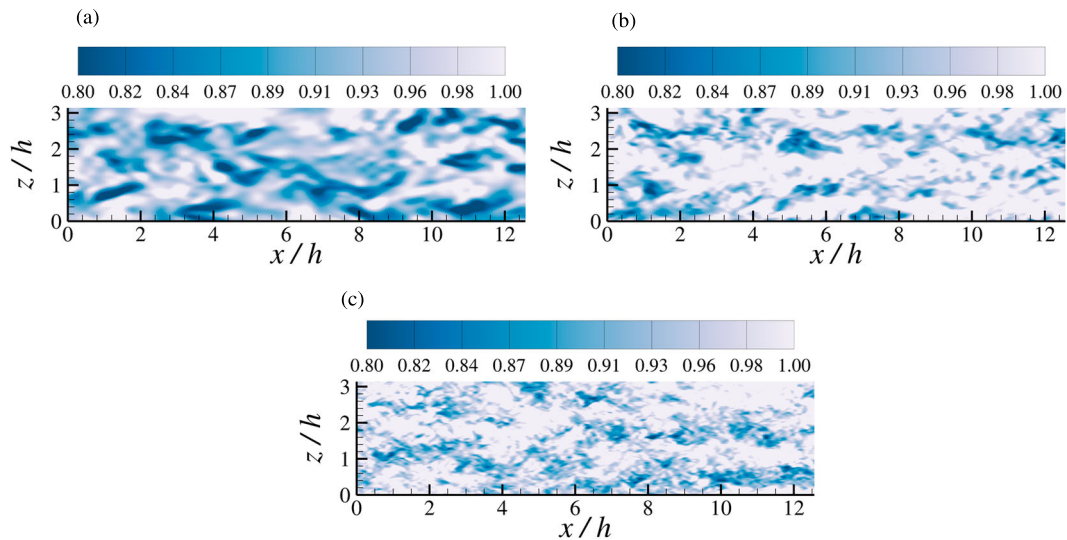


Figure 4 Instantaneous velocity (u/\bar{u}) at the middle of the channel for different Re_τ values: (a) $Re_\tau = 150$, (b) $Re_\tau = 400$, (c) $Re_\tau = 1020$

the streaks become smaller and incoherent. Open-channel flow is different from a boundary-layer flow, as the entrainment of outer irrotational fluid can act as ejections from a wall, thus making the flow closer to that of a closed channel flow (Handler et al., 1993, 1991). At the free surface (Fig. 5) the coherence of the streaks vanish and they become bigger and less elongated. These structures are substantially different from the ones found in the middle of a closed channel flow, and only exist due to the presence of the free surface.

3.3 Two-point correlations and turbulent length scales

Turbulent structures near the free surface are investigated further by examining the two-point correlations and the resulting length scales. These correlations are computed by averaging over all flow realizations and all flow symmetries. Figures 6 and 7 show the two-point correlations in the streamwise and

spanwise directions respectively for the different Re_τ values. Note that the correlations for wall normal and spanwise velocities were also calculated but are not reported in this paper. All the correlations converge to zero, indicating that the domain size is large enough to determine the integral length scales. In the near-wall region ($y^+ \approx 5$), the width of all the correlations decreases as the Re_e number increases, implying smaller length scales. Further away from the wall, ($y^+ \approx 50$), the streamwise correlations are less sensitive to the change in the Re_e number. However, near the free surface the streamwise correlations for $Re_\tau = 400$ and $Re_\tau = 1020$ behave in a similar manner.

The trends of the two-point correlations resulting in the length scales are reported in Fig. 8. Note that in the experimental study of Aubrun, Loyer, Hancock, and Hayden (2013), the length scales were computed by integrating correlation curves up to the first zero crossing. For the current study, the full integral of the correlation curve and also the integral to the first zero

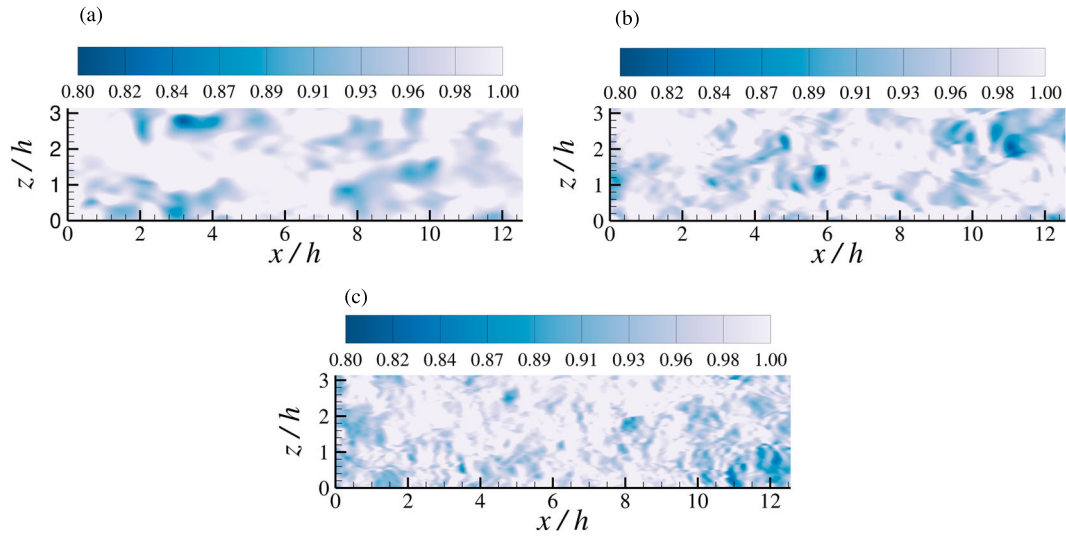


Figure 5 Instantaneous velocity (u/\bar{u}) contours at the free surface for different Re_τ values: (a) $Re_\tau = 150$, (b) $Re_\tau = 400$, (c) $Re_\tau = 1020$

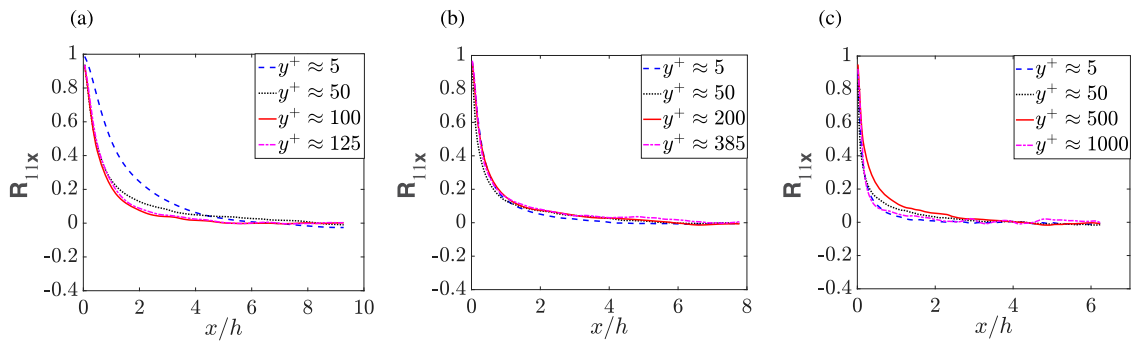


Figure 6 Two-point correlations of streamwise velocities in the streamwise direction (R_{11x}) at different Re_τ and y^+ values: (a) $Re_\tau = 150$, (b) $Re_\tau = 400$, (c) $Re_\tau = 1020$

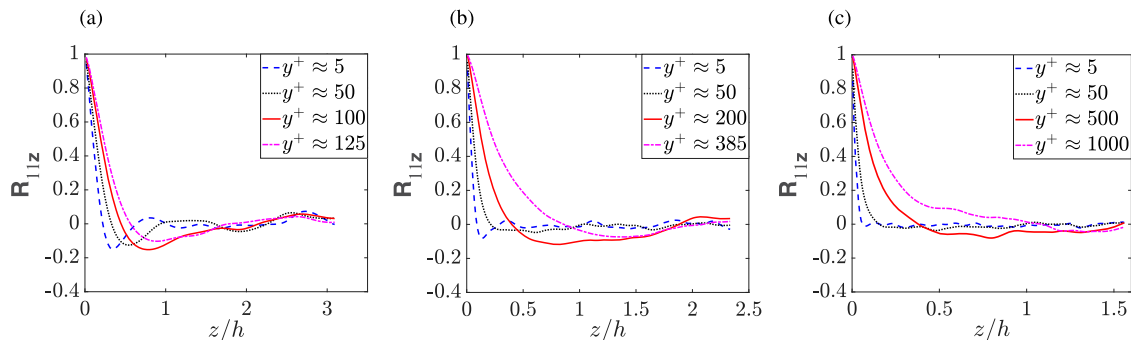


Figure 7 Two-point correlations of streamwise velocities in the spanwise direction (R_{11z}) at different Re_τ and y^+ values: (a) $Re_\tau = 150$, (b) $Re_\tau = 400$, (c) $Re_\tau = 1020$

crossing were calculated. However, no significant difference was found between the results from the two approaches and hence only the profiles from the complete integral of the correlation curves are reported here. The length scales calculated from the u component of velocity in the streamwise direction (L_{11x}) are shown in Fig. 8a. It is observed that in the near-wall region L_{11x} becomes smaller with increasing Re_e numbers. At $Re_\tau = 150$, L_{11x} is largest at the wall and reduces with increasing height (y/h) until the channel mid-depth. After which point the L_{11x} increases again and finally decreases near the free surface. This behaviour is due to the thickness of the viscous

sublayer forming a significant portion of the integral length scale for low Re_e numbers. Similar trends have been reported in the DNS of open-channel flows by Handler et al. (1993) and Handler et al. (1991). L_{11x} for $Re_\tau = 400$ shows similar trends to those of $Re_\tau = 150$, but the effects of the viscous sublayer are reduced, resulting in smaller length scales both at the wall and at the free surface. For the $Re_\tau = 1020$ case, L_{11x} is smallest at the wall and increases with height (y/h) until $y/h \approx 0.9$ and then reduces at the free surface. The near-wall behaviour of L_{11x} is dependent on the Re_e number, but L_{11x} near the free surface is not significantly affected beyond $Re_\tau = 400$.

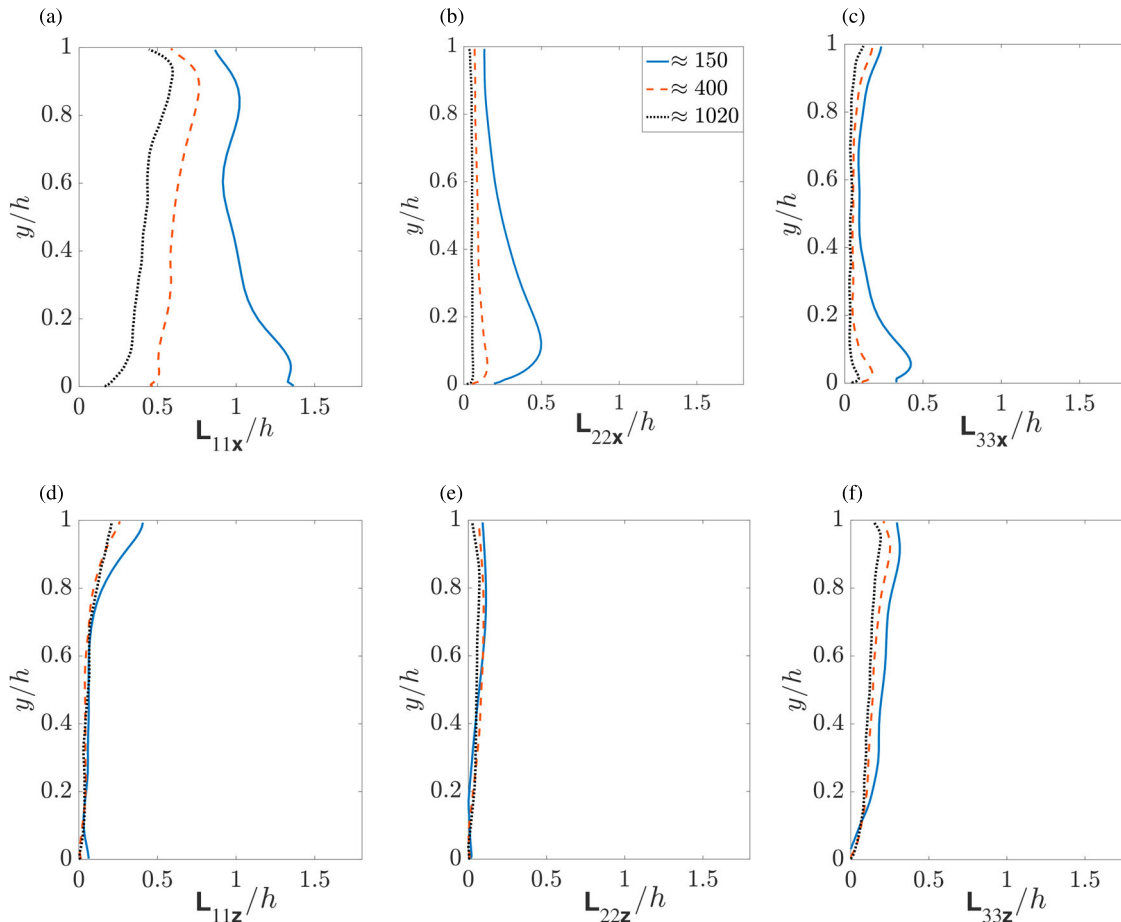


Figure 8 Length scales normalized by the channel height (h) from two-point correlations for $R_{e\tau} = 150$, $R_{e\tau} = 400$ and $R_{e\tau} = 1020$: (a) (L_{11x}/h), (b) (L_{22x}/h), (c) (L_{33x}/h), (d) (L_{11z}/h), (e) (L_{22z}/h), (f) (L_{33z}/h)

The length scales in the streamwise direction for the wall-normal velocity component (L_{22x}) are shown in Fig. 8b. Here L_{22x} decreases with increasing R_e number in the near-wall region. This is associated with the changes in the size of the streaks formed in the near-wall region, as discussed earlier. Note that the $R_{e\tau} = 150$ case has the largest L_{22x} length scale both near the wall and near the free surface. L_{22x} has similar values for the $R_{e\tau}$ of 400 and 1020 near the free surface, signifying that L_{22x} is not significantly affected beyond $R_{e\tau} = 400$.

The length scales in the streamwise direction for the transverse velocity component as reported in Fig. 8c show similar trends as those of L_{11x} and L_{22x} ; decreasing with increasing R_e number. However, near the free surface, the affect of the R_e number once again seems to be insignificant.

The transverse length scales for the streamwise (L_{11z}), wall normal (L_{22z}) and spanwise velocity (L_{33z}) components increase significantly near the free surface ($y/h > 0.8$) for all R_e numbers (Fig. 8d–f). This implies that the transverse length scales become large towards the top of the channel due to the free surface boundary.

Note that the typical size for L_{11x} is of the order of $0.5h - 1h$ and decreases with R_e number. Overall, length scales in the axial direction are largest and the length scales in the wall-normal direction are smallest; i.e. $L_{11} > L_{33} > L_{22}$.

3.4 Reynolds stresses and anisotropy

Figure 9 shows the Reynolds stresses, turbulent kinetic energy and turbulent dissipation profiles in the vertical direction for all the cases. The results in the near-wall region are consistent with those of full-channel flows, whereas there are some deviations from the full-channel flow in the upper part of the channel. These differences are discussed in more detail in Section 3.5. The current numerical profiles have an excellent comparison to the predictions of Yokojima and Shima (2010), in particular near the free-surface region as shown in more detail in the zoom in Fig. 9a. The normalized Reynolds stresses increase with $R_{e\tau}$, as the relative importance of viscosity to momentum transfer diminishes. The free surface has different effects on the normal stresses, with the kinematic boundary condition reducing $\overline{v'v'}$ to zero, whilst $\overline{u'u'}$ and $\overline{w'w'}$ are enhanced. The overall turbulence energy is only modestly affected (Fig. 9e). In contrast to the no-slip wall condition, the non-viscous upper-boundary condition means that the behaviour of stresses is largely independent of the R_e number near the free surface. The influence of the free surface becomes more significant as the R_e number is increased. This is due to the redistribution of the Reynolds stresses by the pressure-strain correlation, which is explained in more detail in Section 3.7. Figure 9f shows that turbulent

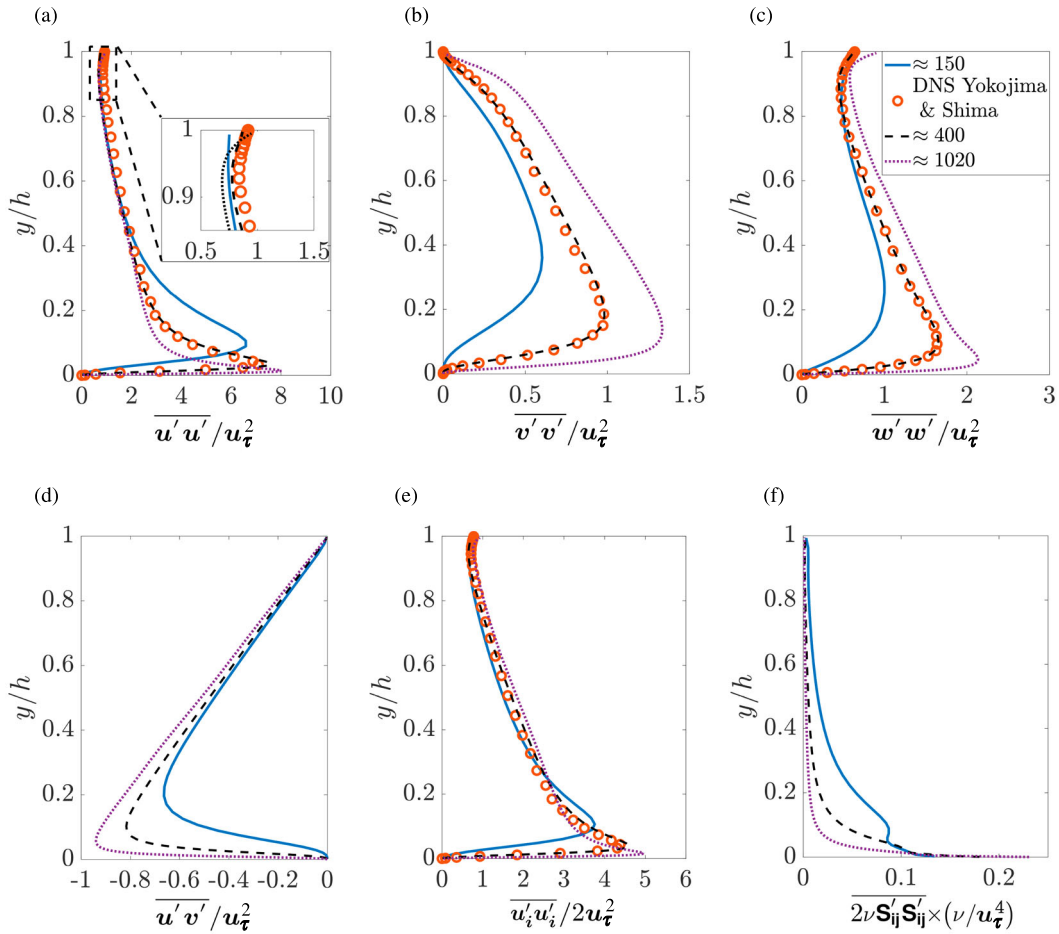


Figure 9 Reynolds stresses and turbulent dissipation for $Re_{\tau} = 150$, $Re_{\tau} = 400$ and $Re_{\tau} = 1020$: (a) $\overline{u'u'}/u_{\tau}^2$, (b) $\overline{v'v'}/u_{\tau}^2$, (c) $\overline{w'w'}/u_{\tau}^2$, (d) $\overline{u'v'}/u_{\tau}^2$, (e) turbulent kinetic energy, (f) turbulent dissipation

dissipation increases at the wall as the Re_e number increases, which is qualitatively consistent with the full-channel flow results of Moser et al. (1999). Turbulent dissipation decreases as the distance from the wall increases, and the rate of decrease is dependent on the Re_e number. This is due to the decrease in the size of the vortical structure in the fluid as the Re_e number increases.

The nature of turbulent structures can be determined by examining the invariants of the anisotropy tensor (Lumley triangle). Anisotropy of the Reynolds stresses near the free surface is the main cause of secondary currents near the free surface in open channel flows (Nakagawa & Nezu, 1993). In the current simulations the level of anisotropy increases in the near-wall and the near-free-surface regions of the flow and the level of anisotropy is dependent on the Re_{τ} of the flow. Readers are encouraged to look at the Lumley triangles and their relevant discussions on the Lumley triangles-Manchester Twiki.⁴

3.5 Comparison of Reynolds stresses with full channel flow

Figures 10 and 11 show the comparison of the Reynolds stresses between the open channel flow and the full channel flow (see figure captions for DNS citations). The Reynolds stresses from

a full channel and open channel flow deviate from each other with an increase in the Re_e number. Note that in the case of open channel flow there is a frictionless rigid lid at $y/h = 1$ where the normal fluctuations are damped leading to zero at the boundary, whereas the fluctuations parallel to the surface are amplified. In the case of full channel this location is at half channel height and there is no restriction on the velocity fluctuations.

At $Re_{\tau} = 150$ the differences between the two channels become apparent near $y/h = 1$ for $\overline{u'u'}$, while significant differences can be seen between $\overline{v'v'}$ and $\overline{w'w'}$ near $y/h = 0.5$ as shown in Fig. 10. In the case of $Re_{\tau} = 400$ the differences in the Reynolds stresses from the two channels appear at $y/h = 0.2$ (plots not shown here). At $Re_{\tau} = 1020$, $\overline{u'u'}$, $\overline{v'v'}$ and $\overline{w'w'}$ are exactly the same in the near-wall region and differences can be seen beyond $y/h = 0.1$ (Fig. 11). Similar differences were noted in the earlier comparison of the two channels at $Re_{\tau} = 590$ by Hinterberger et al. (2008).

3.6 Spectra of velocity

The velocity spectrum tensor $\Phi_{ij}(\kappa)$ represents the Reynolds-stress density in wavenumber space (Pope, 2000). It is required for the calculation of fatigue loading for the design

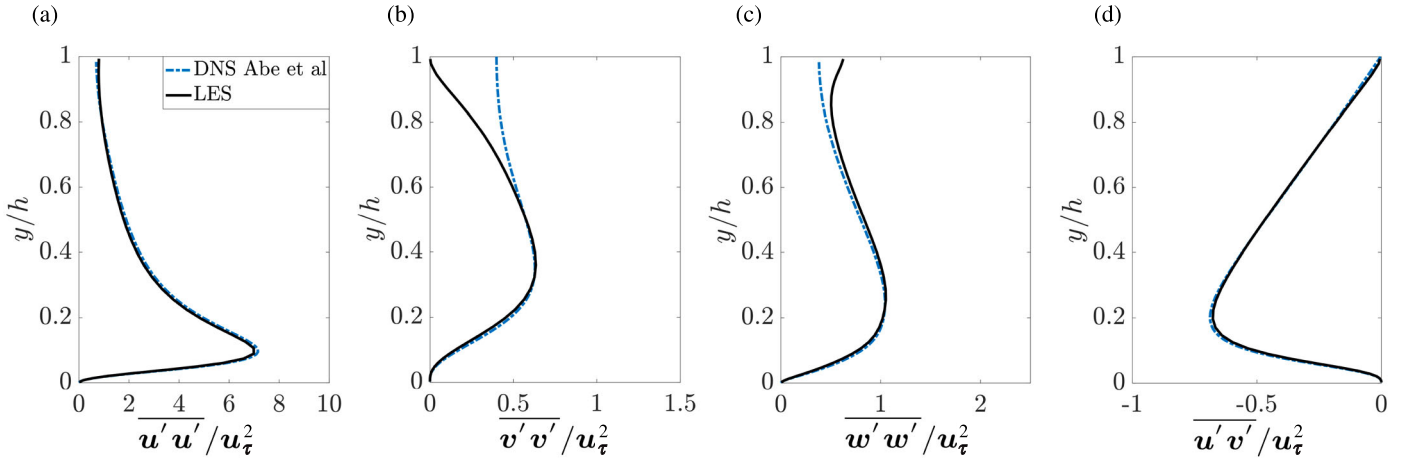


Figure 10 Comparison of Reynolds stresses from LES of open channel flow at $R_{e\tau} = 150$ with DNS data of Abe et al. (2004) for a full channel at $R_{e\tau} = 150$: (a) $\overline{u'u'}/u_\tau^2$, (b) $\overline{v'v'}/u_\tau^2$, (c) $\overline{w'w'}/u_\tau^2$, (d) $\overline{u'v'}/u_\tau^2$

of off-shore structures and marine energy-extraction devices (Milne, Sharma, Flay, & Bickerton, 2013). $\Phi_{ij}(\kappa)$ can be calculated as:

$$\Phi_{ij}(\kappa) = \frac{1}{(2\pi)^3} \int \int_{-\infty}^{\infty} \int \overline{(\mathbf{u}'_i(\mathbf{x})\mathbf{u}'_j(\mathbf{x} + \mathbf{r}))}(\mathbf{r}) \exp(-i\kappa \cdot \mathbf{r}) d\mathbf{r} \quad (3)$$

One-dimensional velocity spectra Φ_{ij} are plotted as a function of the streamwise wave number κ_1 in Fig. 12 for different R_e numbers at different locations in the upper half of the channel. For Φ_{11} and Φ_{33} , there is only a modest variation of energy content with changes in the R_e number, and these are hence not reported here. The most significant influence of the free surface was observed for Φ_{22} (Fig. 12). The energy in the vertical velocity component is preferentially reduced, as only this component is suppressed at the free surface. Similar results have been reported in the earlier studies of Thomas and Hancock (1977), Hannoun, Fernando, and List (1988), Brumley and Jirka (1987), Handler et al. (1993), Handler et al. (1991), Pan and Banerjee (1995) and Calmet and Magnaudet (2003). These trends are also broadly consistent with the predictions of the theory proposed by Hunt and Graham (1978) for the evolution of turbulence near a free surface.

3.7 Budgets for the Reynolds-stress transport equation

In this section the influence of the free surface on the various terms in the Reynolds-stress transport budget is examined. It is important to compare between the low- and high-Reynolds-number cases to differentiate between viscous and inviscid processes and to explain the influence of the anisotropy of the bulk turbulence on the redistribution of energy. At statistically-steady state, the Reynolds-averaged stress-transport equation can be written as:

$$\frac{D\overline{u'_i u'_j}}{Dt} = - \underbrace{\left(\overline{u'_i u'_k} \frac{\partial \overline{u}_j}{\partial x_k} + \overline{u'_j u'_k} \frac{\partial \overline{u}_i}{\partial x_k} \right)}_{\mathbf{P}_{ij}} + \underbrace{\frac{1}{\rho} p' \left(\frac{\partial u'_i}{\partial x_j} + \frac{\partial u'_j}{\partial x_i} \right)}_{\Phi_{ij}}$$

$$\begin{aligned} & - 2\nu \underbrace{\frac{\partial u'_i}{\partial x_k} \frac{\partial u'_j}{\partial x_k}}_{\epsilon_{ij}} + \underbrace{\frac{\partial}{\partial x_k} \left(\nu \frac{\partial u'_i u'_j}{\partial x_k} \right)}_{\mathbf{D}_{ij}^v} \\ & - \underbrace{\frac{\partial}{\partial x_k} \overline{u'_i u'_j u'_k}}_{\mathbf{D}_{ij}^t} - \underbrace{\frac{\partial}{\partial x_k} \left(\frac{1}{\rho} p' \left(u'_i \delta_{jk} + u'_j \delta_{ik} \right) \right)}_{\mathbf{D}_{ij}^p} \end{aligned} \quad (4)$$

where \mathbf{D}_{ij}^p is the production, Φ_{ij} the pressure-strain correlation, ϵ_{ij} the turbulent dissipation, \mathbf{D}_{ij}^v the viscous diffusion, \mathbf{D}_{ij}^t the turbulent diffusion and \mathbf{D}_{ij}^p the pressure diffusion term. Note that the information obtained from these budgets is useful for Reynolds-averaged Navier-Stokes (RANS) modelling, where it is a common practice to modify models for wall-reflection effects. These budgets are thus discussed next.

Total budgets

The total budgets for the normal stress component ($\overline{u'_2 u'_2}$) are presented in Fig. 13 for different R_e numbers; the budgets for $\overline{u'_1 u'_1}$ and $\overline{u'_3 u'_3}$ components are not reported as they are not as significant as budgets of $\overline{u'_2 u'_2}$. The magnitude of \mathbf{P}_{11} , Φ_{11} and ϵ_{11} increases with the R_e number in the near-wall region, as do the diffusion terms (\mathbf{D}_{11}^p , \mathbf{D}_{11}^v and \mathbf{D}_{11}^t). Note that there is no production for the $\overline{u'_2 u'_2}$ component of the Reynolds stress transport equation (i.e. $\mathbf{P}_{22} = 0$). Magnitudes for ϵ_{22} , Φ_{22} and all the diffusion terms (\mathbf{D}_{22}^p , \mathbf{D}_{22}^v and \mathbf{D}_{22}^t) increase with R_e number in the near-wall region, whilst these terms decrease in magnitude near the free surface, as shown in Figs 12–17.

At all R_e numbers, the free surface only contributes to the (2,2) component, most notably with a large negative Φ_{22} pressure correlation component, acting to redistribute energy from $\overline{u'_2 u'_2}$ to the other velocity components. The magnitude of Φ_{22} is, however, significantly smaller near the free surface than near the lower-boundary wall. The effects of the free surface on the individual terms in the Reynolds stress transport equation are examined in detail in the following subsections.

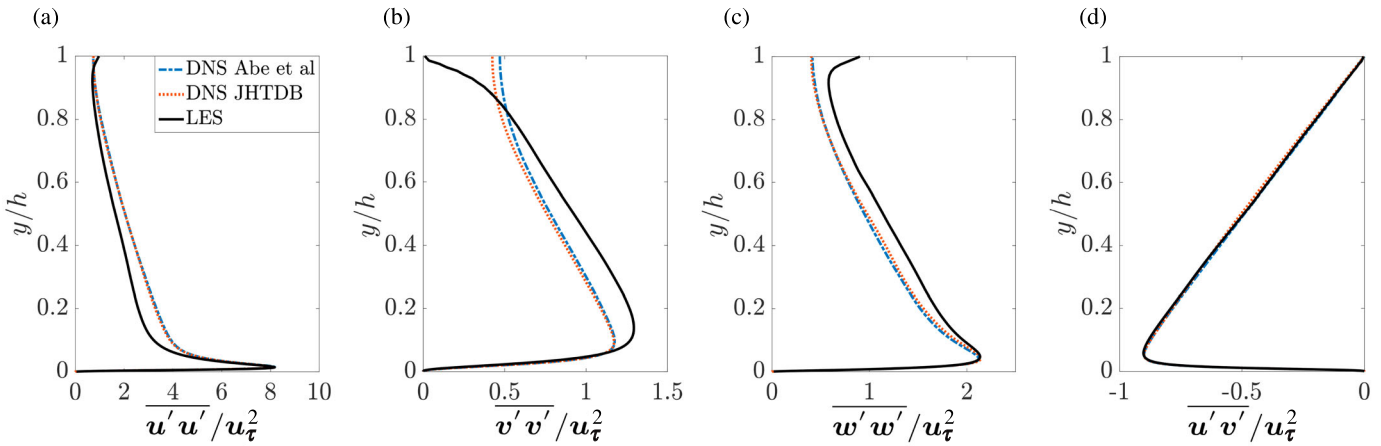


Figure 11 Comparison of Reynolds stresses from LES of open channel flow at $R_{e\tau} = 1020$ with DNS data of Abe et al. (2004) for a full channel at $R_{e\tau} = 1020$ and DNS of a full channel from Johns Hopkins turbulence database Graham et al. (2016) at $R_{e\tau} = 1000$: (a) $\overline{u'u'}/u_\tau^2$, (b) $\overline{v'v'}/u_\tau^2$, (c) $\overline{w'w'}/u_\tau^2$, (d) $\overline{u'v'}/u_\tau^2$

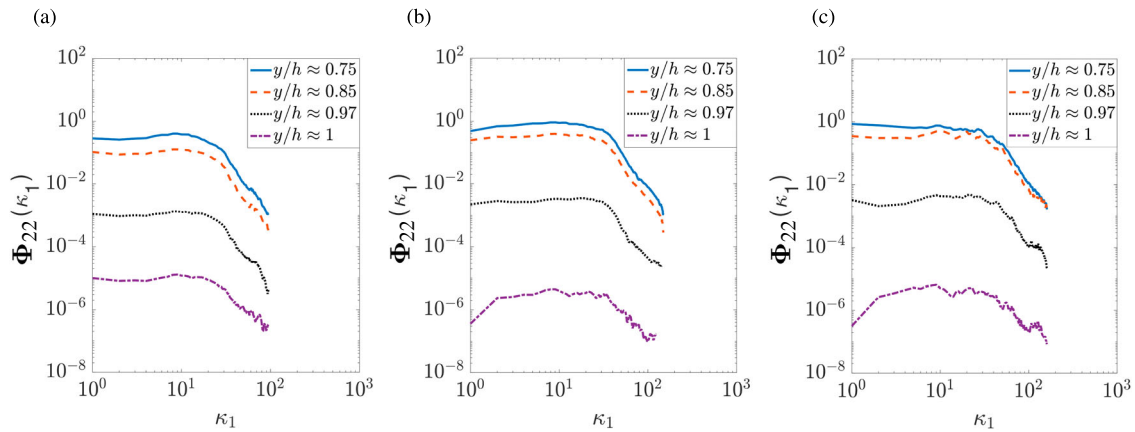


Figure 12 One-dimensional velocity spectra near the free surface at different $R_{e\tau}$ numbers: (a) $R_{e\tau} = 150$, (b) $R_{e\tau} = 400$, (c) $R_{e\tau} = 1020$

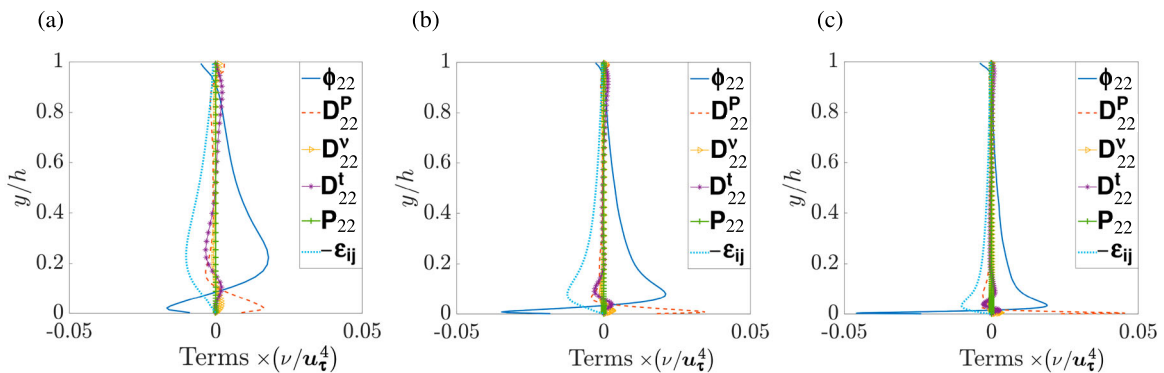


Figure 13 Budgets of wall normal stresses for different $R_{e\tau}$ values normalized by u_τ^4/v : (a) $R_{e\tau} = 150$, (b) $R_{e\tau} = 400$, (c) $R_{e\tau} = 1020$

Production

In fully-developed boundary-layer flows Reynolds stresses are only produced by the \mathbf{P}_{11} and \mathbf{P}_{12} components of the production term, whereas all of the other components are equal to zero. Figure 14 shows that the largest production of Reynolds stresses is near the bottom wall of the channel and the production decreases as the free surface is approached. These results

are consistent with the earlier findings of Taylor et al. (2005), Calmet and Magnaudet (2003) and Yamamoto, Kunugi, and Serizawa (2001). The Reynolds-number dependence on \mathbf{P}_{ij} can be observed by comparing Fig. 14a–c. As the R_e number increases the magnitude of \mathbf{P}_{11} and \mathbf{P}_{12} increases and the influence of \mathbf{P}_{ij} is reduced in the upper half of the channel. This is due to the thinning of the shear layer as the R_e number increases.

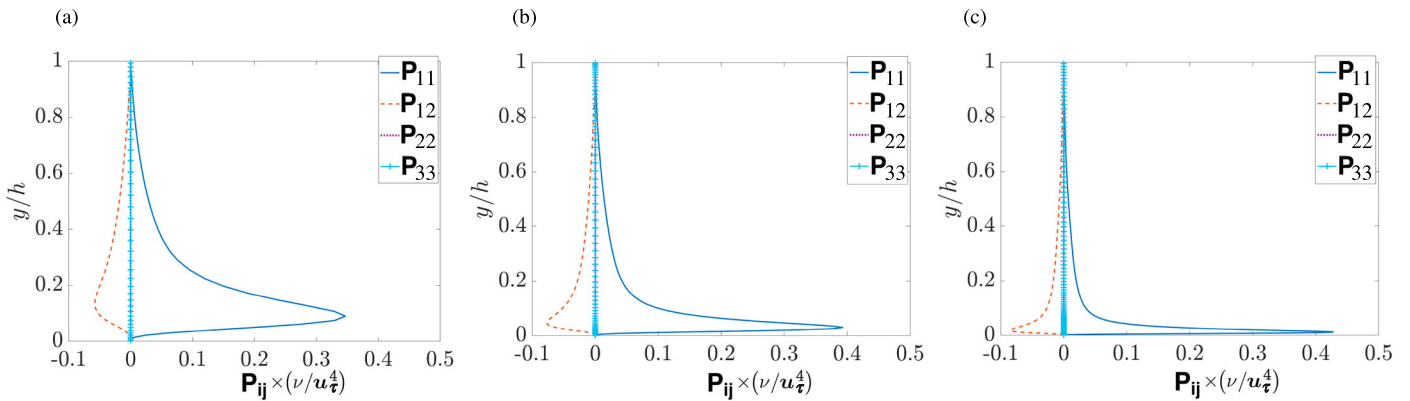


Figure 14 P_{ij} normalized by u_τ^4/ν at different Re_τ values: (a) $Re_\tau = 150$, (b) $Re_\tau = 400$, (c) $Re_\tau = 1020$

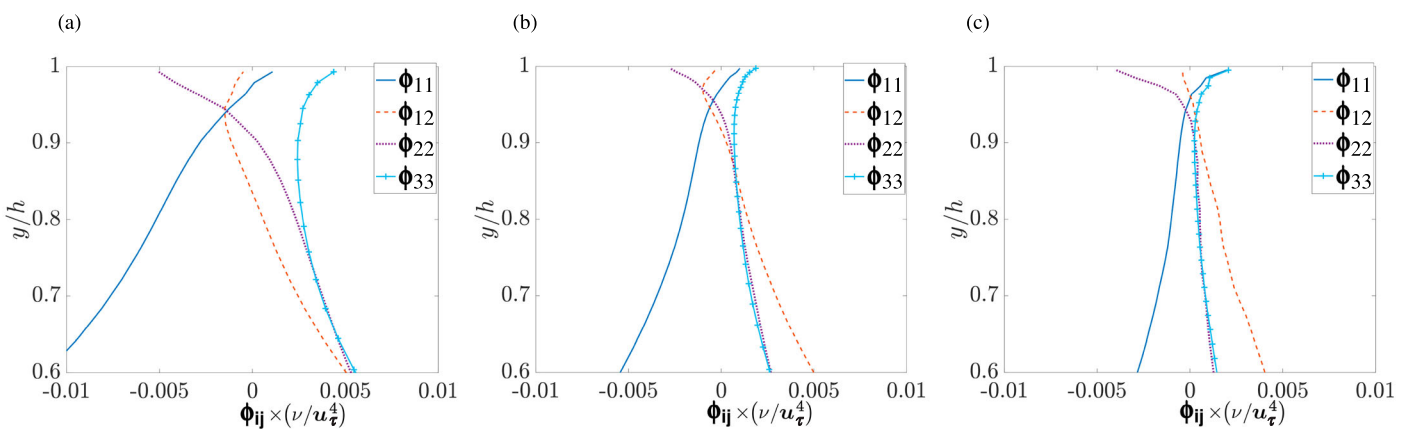


Figure 15 ϕ_{ij} normalized by u_τ^4/ν at different Re_τ values near the free surface: (a) $Re_\tau = 150$, (b) $Re_\tau = 400$, (c) $Re_\tau = 1020$

Pressure–strain correlation

The pressure–strain correlation (ϕ_{ij}) contains pressure fluctuations which have a profound effect on turbulence dynamics. Pressure perturbations travel in all directions as waves through the fluid, and in the case of “incompressible flow” propagate at infinite speed. Thus, pressure effects are not local and are felt instantly across the whole flow domain. In the absence of any boundary, the pressure–strain term reduces the anisotropy which may exist in a turbulent field. In earlier studies it has been recognized that the presence of an impermeable boundary affects not only the normal Reynolds stresses but also the tangential components of the Reynolds stresses. The most common interpretation of this phenomenon is that energy is transferred from the normal component to the tangential ones through pressure–strain correlations (Gibson & Launder, 1978; Launder, Reece, & Rodi, 1975). This implies that ϕ_{ij} tends to increase the local anisotropy in the presence of a boundary. The presence of the free surface introduces anisotropy in the flow field as discussed in Section 3.4.

The value of ϕ_{ij} is very large near the bed of the channel for all Re_e numbers considered in this study, which is consistent with the earlier findings of full channel flows (Hanjalić & Launder, 2011). As the Re_e number is increased, ϕ_{ij} increases, and its influence with height decreases. In Fig. 15 it is observed

that ϕ_{11} , ϕ_{12} , ϕ_{22} and ϕ_{33} are affected by the presence of the free surface. This is due to the restriction of the vertical velocity at the free surface, which causes $\overline{u'_2 u'_2}$ to redistribute its energy to $\overline{u'_1 u'_1}$ and $\overline{u'_3 u'_3}$. Figure 15a–c show that ϕ_{22} is a sink term near the free surface whereas ϕ_{11} and ϕ_{33} are the source terms. Note that the maximum redistribution of ϕ_{22} occurs at the lowest tested Re_e number as the structures from the bed of the channel interact with the free surface. This effect is slightly reduced as the Re_e number increases, as shown in Fig. 15a–c. The Reynolds-number dependence of ϕ_{22} near the free surface has a significant contribution towards the two-component-limit behaviour for open-channel flows.

Pressure diffusion

The pressure diffusion term is recognized as the process which leads to a spatial transport of the Reynolds stresses via the diffusion of the stresses caused by pressure fluctuations. Only D_{12}^P and D_{22}^P contribute to the pressure diffusion in fully-developed boundary-layer flows. Note that D_{ij}^P becomes small as the distance from the wall increases for all Re_e numbers. Figure 16 shows the effects of the free surface on D_{ij}^P , where it is observed that D_{22}^P becomes a source term in the presence of the free surface. Furthermore, these effects decrease with increasing Re_e numbers.

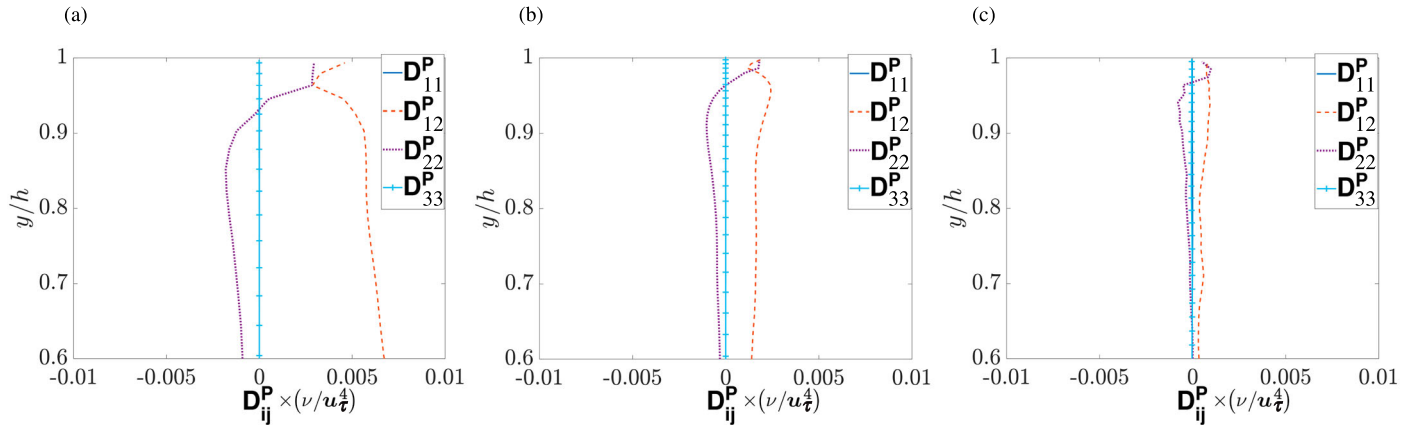


Figure 16 D_{ij}^P normalized by u_τ^4/ν at different Re_τ values near the free surface: (a) $Re_\tau = 150$, (b) $Re_\tau = 400$, (c) $Re_\tau = 1020$

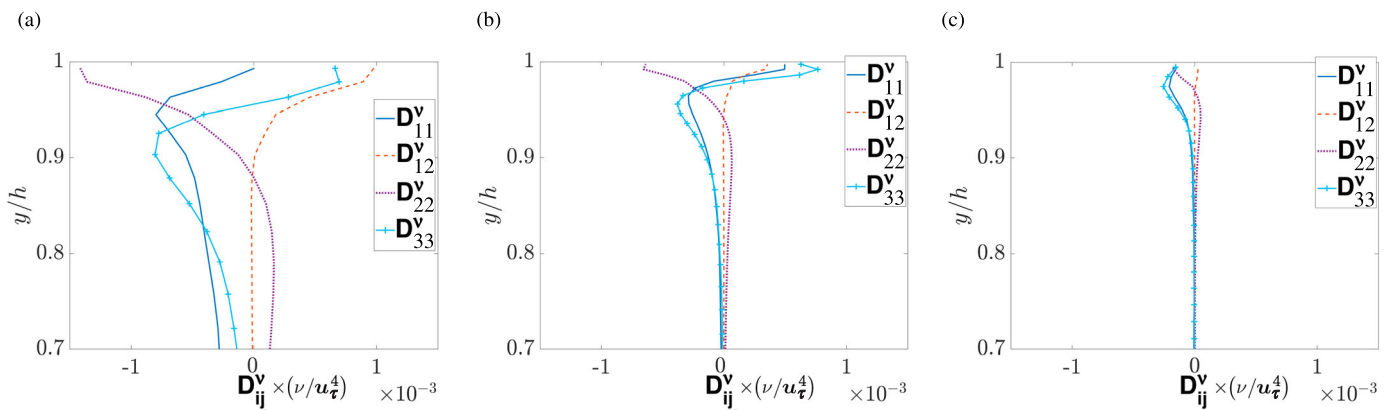


Figure 17 D_{ij}^V normalized by u_τ^4/ν at different Re_τ values near the free surface: (a) $Re_\tau = 150$, (b) $Re_\tau = 400$, (c) $Re_\tau = 1020$

Viscous diffusion

The viscous diffusion term (D_{ij}^V) describes the diffusive transport by molecular action in the Reynolds-stress transport equation. This term is usually very small and is only important in the viscous layer near a wall (Hanjalić & Launder, 2011). It is observed from Fig. 17 that the effect of D_{ij}^V near the free surface decreases with an increase in the Re_e number, that is $D_{ij}^V \rightarrow 0$ near the free surface as $Re_e \rightarrow \infty$.

Diffusion due to triple correlations and turbulent dissipation

The triple correlations (D_{ij}^t) represent the turbulent diffusion of the Reynolds stresses. Plots for diffusion and turbulent dissipation can be accessed via the Diffusion and Turbulent Dissipation-Manchester Twiki link.⁵

Note that the since this is an LES rather than a DNS study, the comparisons, especially near the bottom wall for the turbulent dissipation, are not very accurate and are only presented for qualitative reasons. It is observed from these plots that the influence of the triple-correlation term decreases in the upper half of the channel with increasing Re_e number and the total contribution due to the triple correlations is negligibly small near the free surface. On the other hand ϵ_{ij} represents the effects of turbulent dissipation in the Reynolds-stress transport equation. Note that both the turbulent dissipation and viscous diffusion terms

contain the effects of viscosity. The main difference between the two is that the turbulent dissipation contains the correlations of fluctuating velocity gradients and at the “finest scales of motion” these derivatives are very large. The normal components of turbulence dissipation ϵ_{ii} play a significant role near the bed of the channel, but, due to their viscous nature, become insignificant in the Reynolds-stress budget at greater depths within the channel, including near the free surface (not shown here) (Yamamoto et al., 2001).

4 Summary and conclusions

Large-eddy simulations were performed for fully-developed open-channel flow with a stress-free, impermeable lid. Three Re_e numbers were considered: $Re_\tau = 150, 400, 1020$, based on friction velocity and channel depth. It was found that the mean-velocity profiles agreed well with the open-channel flow results of Taylor et al. (2005) and Nezu and Rodi (1986) at the tested intermediate Re_e number. However, the present study goes beyond these earlier works in terms of the range of the covered Re_e numbers and the turbulence statistics analysis. Normalized mean-velocity profiles also compared well with the channel results of Abe et al. (2004), Moser et al. (1999) and the JHTDB (Graham et al., 2016), admittedly without the more

restrictive upper boundary condition on normal and tangential velocity fluctuations in the present case.

It was observed that the coherent turbulent structures became smaller with an increase in the Reynolds number and incoherent further away from the wall. For the correlations in the streamwise direction, integral length scales for the various velocity components were found to increase in the order streamwise > vertical > spanwise, whilst this order was reversed for correlations in the spanwise direction. The length scales were found to be significantly larger at the lowest tested Re number, but became largely insensitive at the two higher tested Reynolds numbers, except for regions very close to the wall.

For the individual Reynolds stresses, the purely kinematic boundary condition at the free surface distinguishes it from the solid-wall boundary where a no-slip condition is enforced. At the free surface the boundary-normal stress is suppressed, with compensating increases in $\overline{u'u'}$ and $\overline{w'w'}$ maintaining a nearly constant total turbulent kinetic energy. This flattening of eddies was also observed by the approach to the two-component limit indicated by the invariants of the anisotropy tensor, and in the substantial reduction in spectral energy associated with the vertical component in the top 10–15% of the channel. In contrast, there was little effect of the free surface on the spectra of the other velocity components.

In the present study the turbulent transport budgets provided through the supplementary material on the Twiki link⁶ are reported purely for qualitative analysis and flow physics discussions. These budget profiles show that (in a fully-developed flow) the redistribution of turbulence energy from normal to streamwise and spanwise components is overwhelmingly effected by the ϕ_{22} component of the pressure–strain correlation, which goes negative in the upper 5–10% of the channel with equally compensating increases in ϕ_{11} and ϕ_{33} components in the same region to keep the overall pressure–strain correlation traceless. The changes to these components were, however, significantly less than those observed at the lower viscous wall boundary.

The mean-velocity, length scales and Reynolds-stress profiles derived here can (once scaled to appropriate bulk velocity and depth for tidal flows) be used to establish synthetic inlet turbulence conditions for transient analysis such as LES of marine hydrokinetic turbines (see Jarrin et al., 2006, 2009 for synthetic eddy methods). Fluctuating loads for such devices have also recently been analysed by rapid distortion theory by Graham (2017), which gives unsteady pressures around rotor discs; such an approach also requires definition of the onset turbulence. Indeed, LES has already been implemented to compare fluctuating loads with field data for a 1 MW device deployed in the Pentland Firth (Ahmed et al., 2017). Further work is ongoing to establish how realistic channel and tidal-flow turbulence recovers in the wake of such devices and how device performance is affected by free-surface waves. It is also accepted that tidal turbulence will be affected by topographic features, such as headlands, islands, sandbanks, etc.,

but the steady uni-directional case presented here is a valuable reference case.

Funding

The financial support for this work was provided by Engineering and Physical Sciences Research Council (EPSRC) under XMED (EP/J010235/1) and the computational support was provided by the UKTC (under EPSRC grant EP/L000261/1).

Notes

1. Database available online at: <http://www.rs.tus.ac.jp/~t2lab/db/index.html>
2. Database available online at: <http://turbulence.pha.jhu.edu/>
3. Database available online at: https://turbulence.oden.utexas.edu/MKM_1999.html
4. http://cfd.mace.manchester.ac.uk/twiki/pub/CfdTm/TestCase059/Supplementary_Material_for_Twiki.pdf
5. http://cfd.mace.manchester.ac.uk/twiki/pub/CfdTm/TestCase059/Diffusion_and_turbulent_dissipation.pdf
6. http://cfd.mace.manchester.ac.uk/twiki/pub/CfdTm/TestCase059/Supplementary_Material_for_Twiki.pdf

Notation

h	= channel height (m)
p	= pressure (Pa)
\mathbf{r}	= distance vector (m)
t	= time (s)
t_τ	= non-dimensional time (–)
\mathbf{u}_b	= bulk velocity (m s^{-1})
\mathbf{u}_i	= velocity in the i direction (m s^{-1})
$\overline{\mathbf{u}_i' \mathbf{u}_j'}$	= Reynolds stress tensor ($\text{m}^2 \text{s}^{-3}$)
u^+	= non-dimensional velocity (–)
\mathbf{u}_τ	= wall friction velocity (m s^{-1})
y^+	= non-dimensional distance from the wall (–)
x, y, z	= spatial directions (–)
C_f	= skin friction coefficient (–)
C_{sgs}	= Smagorinsky constant (–)
\mathbf{D}_{ij}^p	= pressure diffusion in the Reynolds stress transport equation ($\text{m}^2 \text{s}^{-3}$)
\mathbf{D}_{ij}^v	= viscous diffusion in the Reynolds stress transport equation ($\text{m}^2 \text{s}^{-3}$)
\mathbf{D}_{ij}^t	= diffusion due to triple correlations in the Reynolds stress transport equation ($\text{m}^2 \text{s}^{-3}$)
L_{ij}	= integral length scale in the i and j direction (m)
\mathbf{P}_{ij}	= production term in the Reynolds stress transport equation ($\text{m}^2 \text{s}^{-3}$)
Re	= Reynolds number
Re_τ	= Reynolds number based on the friction velocity (–)
\mathbf{R}_{ij}	= correlation tensor (–)

\mathbf{S}_{ij}	= strain rate tensor (s^{-1})
δ_{ij}	= Kronecker delta
κ	= wavenumber (m^{-1})
η_k	= Kolmogorov scale (m)
ϵ_{ij}	= turbulent dissipation in the Reynolds stress transport equation ($m^2 s^{-3}$)
μ	= fluid dynamic viscosity ($kg m^{-1} s^{-1}$)
μ_{sgs}	= sub-grid-scale viscosity ($kg m^{-1} s^{-1}$)
ν	= fluid kinematic viscosity ($m^2 s^{-1}$)
Φ_{ij}	= pressure–strain correlation in the Reynolds stress transport equation ($m^2 s^{-3}$)
ρ	= density of the fluid ($kg m^{-3}$)
τ_{ij}	= sub-grid-scale stress ($m^2 s^{-2}$)
τ_w	= wall shear stress (Pa)
Δ	= filter width (m)
$\Delta x^+, \Delta y^+, \Delta z^+$	= non-dimensional grid spacing in the x , y and z directions (–)
Φ_{ij}'	= velocity spectrum tensor (–)
\sim	= fluctuating component of a quantity (–)
$\bar{}$	= filtered quantity (–)
$\overline{}$	= Reynolds averaged quantity (–)

ORCID

Umair Ahmed  <http://orcid.org/0000-0002-7828-7895>
 David Apsley  <https://orcid.org/0000-0002-1791-4584>
 Timothy Stallard  <https://orcid.org/0000-0003-2164-1133>
 Peter Stansby  <http://orcid.org/0000-0002-3552-0810>
 Imran Afgan  <https://orcid.org/0000-0002-8082-299X>

References

- Abe, H., Kawamura, H., & Matsuo, Y. (2004). Surface heat-flux fluctuations in a turbulent channel flow up to $Re_\tau = 1020$ with $Pr = 0.025$ and 0.71 . *International Journal of Heat and Fluid Flow*, 25(3), 404–419.
- Ahmed, U., Apsley, D. D., Afgan, I., Stallard, T., & Stansby, P. (2017). Fluctuating loads on a tidal turbine due to velocity shear and turbulence: Comparison of CFD with field data. *Renewable Energy*, 112(2017), 235–246.
- Ahmed, U., & Prosser, R. (2018). A Posteriori assessment of algebraic scalar dissipation models for RANS simulation of premixed turbulent combustion. *Flow, Turbulence and Combustion*, 100(1), 39–73.
- Archambeau, F., Mechtoua, N., & Sakiz, M. (2004). A finite volume method for the computation of turbulent incompressible flows - industrial applications. *International Journal on Finite Volumes*, 1, 1–62.
- Aubrun, S., Loyer, S., Hancock, P. E., & Hayden, P. (2013). Wind turbine wake properties: Comparison between a non-rotating simplified wind turbine model and a rotating model. *Journal of Wind Engineering and Industrial Aerodynamics*, 120, 1–8.
- Borue, V., Orszag, S. A., & Staroselsky, I. (1995). Interaction of surface waves with turbulence: Direct numerical simulations of turbulent open-channel flow. *Journal of Fluid Mechanics*, 286, 1–23.
- Brodkey, R. S., Wallace, J. M., & Eckelmann, H. (1974). Some properties of truncated turbulence signals in bounded shear flows. *Journal of Fluid Mechanics*, 63(2), 209.
- Brumley, B. H., & Jirka, G. H. (1987). Near-surface turbulence in a grid-stirred tank. *Journal of Fluid Mechanics*, 183(1), 235–263.
- Calmet, I., & Magnaudet, J. (2003). Statistical structure of high-Reynolds-number turbulence close to the free surface of an open-channel flow. *Journal of Fluid Mechanics*, 474, 355–378.
- Campagne, G., Cazalbou, J.-B., Joly, L., & Chassaing, P. (2009). The structure of a statistically steady turbulent boundary layer near a free-slip surface. *Physics of Fluids*, 21(6), 065111.
- Gibson, M. M., & Launder, B. (1978). Ground effects on pressure fluctuations in the atmospheric boundary layer. *Journal of Fluid Mechanics*, 86(pt 3), 491–511.
- Graham, J., Kanov, K., Yang, X. I. A., Lee, M., Malaya, N., Lalescu, C. C., & Meneveau, C. (2016). A Web services accessible database of turbulent channel flow and its use for testing a new integral wall model for LES. *Journal of Turbulence*, 17(2), 181–215.
- Graham, J. M. R. (2017). Rapid distortion of turbulence into an open turbine rotor. *Journal of Fluid Mechanics*, 825, 764–794.
- Handler, R. A., Swean, T. F., Leighton, R. I., & Swearingen, J. D. (1993). Length scales and the energy balance for turbulence near a free surface. *AIAA Journal*, 31(11), 1998–2007.
- Handler, R. A., Swearingen, J. D., Swean, T. F., & Leighton, R. I. (1991). Length scales of turbulence near a free surface. *22nd Fluid Dynamics, Plasma Dynamics and Lasers Conference*, Honolulu, Hawaii. American Institute of Aeronautics and Astronautics.
- Hanjalić, K., & Launder, B. (2011). *Modelling turbulence in engineering and the environment (Second-moment routes to closure)*. Cambridge: Cambridge University Press.
- Hannoun, I. A., Fernando, H. J. S., & List, E. J. (1988). Turbulence structure near a sharp density interface. *Journal of Fluid Mechanics*, 189(1988), 189–209.
- Hinterberger, C., Fröhlich, J., & Rodi, W. (2008). 2D and 3D turbulent fluctuations in open channel flow with $Re_\tau = 590$ studied by Large Eddy simulation. *Flow, Turbulence and Combustion*, 80(2), 225–253.
- Hunt, J. C. R., & Graham, J. M. R. (1978). Free-stream turbulence near plane boundaries. *Journal of Fluid Mechanics*, 84(2), 209–235.
- Jarrin, N., Benhamadouche, S., Laurence, D. R., & Prosser, R. (2006). A synthetic-eddy-method for generating inflow

- conditions for large-eddy simulations. *International Journal of Heat and Fluid Flow*, 27, 585–593.
- Jarrin, N., Prosser, R., Uribe, J. C., Benhamadouche, S., & Laurence, D. R. (2009). Reconstruction of turbulent fluctuations for hybrid RANS/LES simulations using a Synthetic-Eddy method. *International Journal of Heat and Fluid Flow*, 30(3), 435–442.
- Kim, J., Moin, P., & Moser, R. D. (1987). Turbulence statistics in fully developed channel flow at low Reynolds number. *Journal of Fluid Mechanics*, 177, 133–166.
- Kline, S. J., Reynolds, W. C., Schraub, F. A., & Runstadler, P. W. (1967). The structure of turbulent boundary layers. *Journal of Fluid Mechanics*, 30(4), 741–773.
- Komori, S., Murakami, Y., & Ueda, H. (1989). The relationship between surface-renewal and bursting motions in an open-channel flow. *Journal of Fluid Mechanics*, 203(1989), 103–123.
- Komori, S., Nagaosa, R., Murakami, Y., Chiba, S., Ishii, K., & Kuwahara, K. (1993). Direct numerical simulation of three-dimensional open-channel flow with zero-shear gas-liquid interface. *Physics of Fluids A: Fluid Dynamics*, 5(1), 115–125.
- Komori, S., Ueda, H., Ogino, F., & Tokuro, M. (1982). Turbulence structure and transport mechanism at the free surface in an open channel flow. *International Journal of Heat and Mass Transfer*, 25(4), 513–521.
- Kumar, S., Gupta, R., & Banerjee, S. (1998). An experimental investigation of the characteristics of free-surface turbulence in channel flow. *Physics of Fluids*, 10(2), 437–456.
- Lam, K., & Banerjee, S. (1992). On the condition of streak formation in a bounded turbulent flow. *Physics of Fluids A: Fluid Dynamics*, 4(2), 306–320.
- Launder, B., Reece, G. J., & Rodi, W. (1975). Progress in the development of a Reynolds-stress turbulence closure. *Journal of Fluid Mechanics*, 68(3), 537–566.
- Milne, I. A., Sharma, R. N., Flay, R. G. J., & Bickerton, S. (2013). Characteristics of the turbulence in the flow at a tidal stream power site. *Philosophical Transactions of the Royal Society A: Mathematical, Physical and Engineering Sciences*, 371(1985), 20120196–20120196.
- Moser, R. D., Kim, J., & Mansour, N. N. (1999). Direct numerical simulation of turbulent channel flow up to $Re_\tau = 590$. *Physics of Fluids*, 11(4), 943–945.
- Nakagawa, H., & Nezu, I. (1981). Structure of space-time correlations of bursting phenomena in an open-channel flow. *Journal of Fluid Mechanics*, 104, 1–43.
- Nakagawa, H., & Nezu, I. (1993). *Turbulence in open channel flows (IAHR monographs)*. Rotterdam.
- Nezu, I., & Rodi, W. (1986). Open-channel flow measurements with a laser Doppler anemometer. *Journal of Hydraulic Engineering*, 112(5), 335–355.
- Pan, Y., & Banerjee, S. (1995). A Numerical Study of Free-Surface Turbulence in Channel Flow. *Physics of Fluids*, 7(7), 1649–1664.
- Pope, S. B. (2000). *Turbulent flows*. Cambridge: Cambridge University Press.
- Rashidi, M., & Banerjee, S. (1988). Turbulence structure in free-surface channel flows. *Physics of Fluids*, 31(9), 2491–2503.
- Roussinova, V., Balachandar, R., & Biswas, N. (2009). Reynolds stress anisotropy in open-channel flow. *Journal of Hydraulic Engineering*, 135(10), 812–824.
- Salveti, M. V., Zang, Y., Street, R. L., & Banerjee, S. (1997). Large-eddy simulation of free-surface decaying turbulence with dynamic subgrid-scale models. *Physics of Fluids*, 9(8), 2405–2419.
- Sillero, J. A., Jiménez, J., & Moser, R. D. (2014). Two-point statistics for turbulent boundary layers and channels at Reynolds numbers up to $\delta^+ = 2000$. *Physics of Fluids*, 26(10), 105109.
- Smagorinsky, J. (1963). General circulation experiments with the primitive equations. *Monthly Weather Review*, 91(3), 99–164.
- Taylor, J. R., Sarkar, S., & Armenio, V. (2005). Large eddy simulation of stably stratified open channel flow. *Physics of Fluids*, 17(11), 1–18.
- Thomas, N. H., & Hancock, P. E. (1977). Grid turbulence near a moving wall. *Journal of Fluid Mechanics*, 82(3), 481–496.
- Walker, D. T., Leighton, R. I., & Garza-Rios, L. O. (1996). Shear-free turbulence near a flat free surface. *Journal of Fluid Mechanics*, 320(1), 19.
- Walker, R., Tejada-Martínez, A., Martinat, G., & Grosch, C. (2014). Large-eddy simulation of open channel flow with surface cooling. *International Journal of Heat and Fluid Flow*, 50, 209–224.
- Yamamoto, Y., Kunugi, T., & Serizawa, A. (2001). Turbulence statistics and scalar transport in an open-channel flow. *Journal of Turbulence*, 2(789305785), N10.
- Yokojima, S., & Shima, N. (2010). Applicability of elliptic-relaxation method to free-surface turbulence. *Fluid Dynamics Research*, 42(3), 035505.